Research Square

Preprints are preliminary reports that have not undergone peer review.
They should not be considered conclusive, used to inform clinical practice,
or referenced by the media as validated information.

Germline TWAS Convergence Between NMN-Responsive Aging Pathways and Triple-Negative Breast Cancer Susceptibility: Autophagy and MAP2K2 as Translational Leads

Ngo Cheung

info@cheungngomedical.com

Independent Researcher

Research Article

Keywords: triple-negative breast cancer, TWAS, S-PrediXcan, autophagy, MAP2K2, nicotinamide mononucleotide, NAD-positive metabolism, endocytosis, CPT2

Posted Date: September 10th, 2026

DOI: https://doi.org/10.21203/rs.3.rs-10375315/v1

License: This work is licensed under a Creative Commons Attribution 4.0 International License.
Read Full License

Additional Declarations: No competing interests reported.

Abstract

Background

Triple-negative breast cancer remains difficult to prevent and treat because it lacks the receptor-defined targets available for other breast cancer subtypes and encompasses considerable biological heterogeneity. Autophagy, NAD-positive metabolism, and intracellular trafficking help cells adapt to metabolic stress and age-related damage. Long-term nicotinamide mononucleotide treatment in mice has also been linked to transcriptional changes involving RAB11A-mediated trafficking, CPT2-dependent fatty-acid oxidation, MAP2K2 signaling, and autophagy-related processes. Whether these pathways overlap with inherited susceptibility to triple-negative breast cancer is unknown.

Methods

A multi-gene-set transcriptome-wide association study pipeline was applied to overall breast cancer and triple-negative breast cancer summary statistics derived from Zhang et al. (2020). Ten full KEGG pathways nominated through 35 NMN-responsive genes were evaluated using tissue-combined S-PrediXcan scores, Stouffer enrichment, random-gene permutation, bootstrap confidence intervals, differential tests, cross-phenotype profile correlations, leave-one-out influence analysis, and sensitivity analyses.

Results

Autophagy produced the strongest supported result in triple-negative breast cancer, with a Stouffer Z of −8.98, a bootstrap 95% confidence interval of −14.78 to −3.09, a permutation p value of .0022, and a pathway false discovery rate of .022. The overall breast cancer–triple-negative breast cancer difference was consistent across 11 tissues, with a mean gap of +2.83 and the same gap direction in 82% of tissues. The signal remained stable under the prespecified influence rule. MAP2K2 was recurrent across autophagy, Ras/MAPK, and cytoskeletal pathways and had oppositely signed associations in the two phenotypes. Endocytosis was suggestive but did not survive pathway correction. Fatty-acid degradation was not enriched but showed marked cross-phenotype anticorrelation.

Conclusions

The results identify an autophagy-related germline expression pattern associated with triple-negative breast cancer susceptibility and nominate MAP2K2 for focused follow-up. They support cross-context convergence between NMN-responsive aging biology and breast cancer genetics, but they do not show that NMN prevents or treats breast cancer. Gene-level colocalization, case-case analyses, and functional validation are required.

Introduction

Triple-negative breast cancer is defined clinically by the absence of estrogen receptor, progesterone receptor, and human epidermal growth factor receptor 2 expression or amplification. This definition is useful in practice, but it combines tumors with different molecular programs, immune environments, metabolic states, and treatment sensitivities. Although immunotherapy, poly(ADP-ribose) polymerase inhibitors, and antibody–drug conjugates have broadened treatment options, TNBC still has fewer widely applicable receptor-directed strategies than hormone receptor-positive or HER2-positive disease. It also tends to present with more aggressive clinical features and an earlier risk of recurrence. These difficulties have encouraged a search for markers that identify subtype vulnerability before tumor development and for biological processes that can separate clinically meaningful TNBC groups [1].

Germline studies show that breast cancer subtypes do not share an identical inherited architecture. Zhang et al. [2] analyzed 133,384 breast cancer cases and 113,789 controls, together with data from BRCA1 mutation carriers, and identified 32 previously unreported susceptibility loci. Fifteen showed evidence of heterogeneity by at least one tumor feature, and five had associations in opposite directions between luminal and non-luminal disease. Genetic correlations among five intrinsic-like subtypes ranged from 0.35 to 0.80. The proportion of chip heritability explained by known susceptibility loci was also lower for triple-negative disease than for luminal A-like disease, at 37.6% and 54.2%, respectively. These observations provide a clear reason to examine subtype-specific biology rather than assuming that an association with breast cancer overall applies equally to TNBC.

Metabolic adaptation is one possible source of subtype heterogeneity. Cancer cells must maintain energy production, membrane synthesis, redox balance, protein quality control, and organelle function under conditions that may include hypoxia and limited nutrient availability. These pressures intersect with several processes that change during aging. Cellular NAD-positive availability, mitochondrial function, stress signaling, protein turnover, and autophagy are all altered with age, although their direction and importance differ by tissue and physiological context [3, 4]. Such overlap does not mean that aging and cancer are equivalent states. It does, however, raise the possibility that inherited regulation of pathways involved in metabolic aging may influence which breast cancer subtype develops.

Nicotinamide mononucleotide is an intermediate in NAD-positive biosynthesis. In aged mice, long-term NMN administration mitigated several physiological changes, including disturbances in energy metabolism and insulin sensitivity, without establishing an anticancer effect [5]. NAD-positive availability can influence sirtuin activity, while AMPK and mTOR signaling regulate the initiation of autophagy through ULK1. SIRT1 can also interact with components of the autophagy machinery [6, 7]. These links are context dependent. NMN exposure cannot be assumed to activate the same pathways in every tissue, and a metabolic response in normal aged tissue cannot be transferred directly to a tumor.

A reanalysis of the Mills et al. dataset identified 35 genes whose age-associated expression patterns were reported to be rescued by NMN in at least two of three metabolic tissues: skeletal muscle, liver, and white adipose tissue [8]. Twenty-six genes showed directionally consistent rescue across the tissues in which they met the selection criteria, whereas nine were discordant. No gene was rescued in all three

tissues. The underlying experiment had four mice per group, and no individual gene survived genome-wide multiple-testing correction. The 35-gene set should therefore be regarded as a structured source of hypotheses rather than a definitive NMN transcriptional signature.

Several genes from that analysis had clear links to established pathways. RAB11A, the highest-priority candidate in the preprint, was associated with endosomal recycling and trafficking. CPT2 was the only mitochondrial gene in the robust set and provided a direct link to long-chain fatty-acid oxidation. MAP2K2 connected the set to Ras–RAF–MEK–ERK signaling, while the mouse Trp53inp2 signal mapped to the human autophagy gene TP53INP2. Other candidates included GALR1, SLC13A5, APBA2, MYO15, ACD, WAP, ZFAND2B, BCHE, DUSP11, FMO2, PKNOX1, PSME3, RANGAP1, SPG21, and SYNGR2, together with several olfactory receptor, RIK, and uncharacterized loci. The less well-annotated genes had limited representation in standard human KEGG pathways.

Mapping the NMN-responsive genes nominated ten KEGG pathways: autophagy–animal, endocytosis, fatty-acid degradation, MAPK signaling, Ras signaling, PPAR signaling, neuroactive ligand–receptor interaction, regulation of the actin cytoskeleton, the citrate cycle, and the synaptic vesicle cycle. This mapping does not imply that every member of these pathways responded to NMN. It identifies broader biological systems containing one or more genes from the 35-gene list.

Autophagy was of particular interest because it lies at the boundary between cellular maintenance and cancer adaptation. The pathway removes damaged proteins and organelles and recycles intracellular material through lysosomal degradation. In early tumor development, effective autophagy can limit oxidative damage, inflammation, and genome instability. In established cancers, the same recycling system may help malignant cells survive starvation, hypoxia, and treatment. Its effects therefore depend on the timing, tissue, genotype, and state of the tumor [9–12]. Breast cancer studies likewise show that autophagy markers and dependencies vary among molecular subtypes [13, 14].

The present study asked whether the full KEGG pathways nominated by the NMN-responsive gene set show inherited expression associations with overall breast cancer or TNBC. It also asked whether their gene-level TWAS profiles differ between the two phenotypes and whether individual NMN-nominated genes emerge as plausible bridges between aging metabolism and subtype susceptibility. The analysis was designed as a pathway-convergence study, not as a test of NMN treatment. Its main constraints were defined in advance: the pathways were much larger than the original 35-gene set, TNBC was nested within the overall breast cancer resource, and a TWAS score concerns genetically predicted expression rather than expression measured in a tumor.

Methods

Data sources

The breast cancer association data were derived from the overall and subtype-specific analyses reported by Zhang et al. [2] (Fig. 1). The source study included breast cancers recorded as invasive, in situ, or of

unknown invasiveness in the overall analysis and used tumor characteristics including estrogen receptor, progesterone receptor, HER2 status, and grade to study subtype heterogeneity. Its TNBC analysis used data from the Breast Cancer Association Consortium and the Consortium of Investigators of Modifiers of BRCA1/2. The overall and TNBC datasets were therefore not independent. Some cases and controls contributed to related analyses, and TNBC cases formed part of the wider breast cancer population.

The supplied TWAS outputs had been generated with S-PrediXcan models based on GTEx v8 expression reference data. S-PrediXcan estimates the association between the genetically regulated component of gene expression and a GWAS phenotype using summary statistics [15, 16]. Eleven tissues were available: subcutaneous adipose, visceral omental adipose, breast mammary tissue, EBV-transformed lymphocytes, cultured fibroblasts, liver, ovary, spleen, uterus, vagina, and whole blood.

For each phenotype, files were read using gene symbols or Ensembl identifiers and their corresponding S-PrediXcan Z scores. Symbols were converted to uppercase, Ensembl version suffixes were removed when necessary, and duplicate rows within a tissue were reduced to the first occurrence. When both an Ensembl identifier and a gene symbol were present, the symbol served as the canonical name.

NMN-derived pathway selection

The pathway hypotheses came from the 35 cross-tissue genes reported in the reanalysis of the long-term NMN mouse experiment [8, 5]. The principal genes used to guide interpretation were RAB11A, CPT2, MAP2K2, GALR1, SLC13A5, APBA2, and TP53INP2. The last of these requires species-aware nomenclature: Trp53inp2 is the mouse-style symbol, whereas TP53INP2 is the recognized human symbol. The original Stage 3 interest list used “TRP53INP2,” which prevented exact matching to the human TWAS symbol and slightly undercounted the overlap between the nominated genes and the autophagy pathway.

The ten analyzed gene sets were the complete human KEGG pathways for autophagy–animal, endocytosis, fatty-acid degradation, MAPK signaling, Ras signaling, PPAR signaling, neuroactive ligand–receptor interaction, regulation of the actin cytoskeleton, the citrate cycle, and the synaptic vesicle cycle. These were not restricted to the intersection between KEGG and the 35 NMN-responsive genes. The analysis therefore tested whether broad pathways nominated by the NMN study were enriched in breast cancer TWAS associations.

Tissue and pathway meta-analysis

For each gene, tissue-specific S-PrediXcan Z scores were combined as the sum of the available tissue Z scores divided by the square root of the number of contributing tissues. The resulting value was treated as a cross-tissue gene-level meta-Z. This procedure gives equal weight to all available tissues and assumes approximate independence, although GTEx prediction models and the underlying GWAS associations are correlated across tissues.

For each KEGG pathway, available gene meta-Z scores were combined using the same Stouffer form. In the prespecified robust mode, gene-level values were winsorized at the first and 99th percentiles before calculation of the pathway Stouffer Z, mean Z, and mean absolute Z. Median and trimmed-mean statistics were also recorded. Coverage was defined as the proportion of pathway genes with an available TWAS score.

A two-sided Wilcoxon signed-rank test evaluated whether pathway gene Z scores were centered on zero. Competitive permutation testing drew random gene sets of the same size without replacement from all genes available for the phenotype. Ten thousand random sets were used, and the empirical p value was calculated from the absolute Stouffer statistic. Bootstrap confidence intervals were generated from 2,000 gene-level resamples with replacement. False discovery rates for pathway enrichment were calculated across the ten pathways within each phenotype using the Benjamini–Hochberg method.

Cross-phenotype comparisons and sensitivity analyses

Comparisons between overall breast cancer and TNBC were restricted to pathway genes available for both phenotypes. Distributional differences were assessed with Mann–Whitney, Kolmogorov–Smirnov, Welch, Brunner–Munzel, paired t, and paired Wilcoxon tests. Cohen's d, rank-biserial correlation, sign concordance, Kendall correlation, Lin's concordance coefficient, and sign-flip permutation results were also recorded. Global false discovery rates were calculated across the ten gene sets for each family of pairwise tests.

Profile similarity was evaluated using Pearson, Spearman, cosine, Euclidean, and Manhattan measures. Because genes within pathways may share expression predictors, genomic regions, and regulatory variants, the nominal correlation p values were treated as descriptive evidence rather than independent gene-level tests.

Leave-one-out influence analysis recalculated the pathway Stouffer statistic after removing one gene at a time. A gene was flagged if removal changed the pathway statistic by more than 20% or reversed its sign. This relative threshold becomes unstable when the original pathway Z is close to zero. The number of flagged genes was therefore not interpreted as a count of biological discoveries. A secondary sensitivity analysis removed all flagged genes and recalculated the raw, non-winsorized Stouffer statistic. Retention of an absolute Z above 1.96 was considered threshold stability, not proof of corrected pathway enrichment.

The pipeline also generated a pooled Benjamini–Hochberg adjustment across enrichment, differential, proximity, and concordance tests. Although the output was labeled "family-wise FDR," it was a pooled global FDR procedure rather than control of the family-wise error rate. Its results were considered supplementary because the pool included correlated and partly duplicated tests.

Interpretation

Under standard S-PrediXcan coding and correct allele harmonization, a negative gene Z indicates that higher genetically predicted expression is associated with lower odds of the phenotype, while a positive Z indicates association with higher odds. A pathway Stouffer Z summarizes the net direction across genes and does not mean that every gene has the same effect. It also does not measure RNA expression in breast tumors or establish a change in autophagic flux.

TWAS associations can arise from a causal expression mechanism, linkage disequilibrium with another causal signal, or horizontal pleiotropy. Colocalization and conditional analyses are needed before assigning a causal role to an individual gene [17].

Results

Overview

All ten KEGG pathways had sufficient coverage for cross-phenotype analysis. Coverage in the leading pathways was generally high, reaching 90% for TNBC autophagy and 96% for TNBC endocytosis. Autophagy received the highest custom Stage 3 priority score, 0.728, followed by endocytosis at 0.304. This score combined pathway divergence, maximum absolute Z, overlap with nominated NMN genes, and permutation FDR. It was used for ranking only and had no formal inferential meaning. The pathway ranking is shown in Table 1.

Seven pathways had significant negative correlations between their overall breast cancer and TNBC TWAS profiles under the nominal profile tests. The strongest Pearson correlation was observed for fatty-acid degradation, followed by the synaptic vesicle cycle, neuroactive ligand–receptor interaction, autophagy, endocytosis, and PPAR signaling. Ras signaling crossed the prespecified threshold using Spearman rather than Pearson correlation. The uniform direction of these correlations raised the possibility of subtype heterogeneity but also made sign harmonization and genome-wide comparison important follow-up checks.

Table 1
Composite pathway prioritization

Rank	Gene set	Score	Divergence	Maximum absolute Z	Interest overlap	Best FDR
1	KEGG AUTOPHAGY ANIMAL	0.728	1.09	8.98	1%	0.022
2	KEGG ENDOCYTOSIS	0.304	0.39	5.68	0%	0.2085
3	KEGG NEUROACTIVE LIGAND RECEPTOR INTERACTION	0.180	0.38	3.50	0%	0.7437
4	KEGG REGULATION OF ACTIN CYTOSKELETON	0.166	0.36	2.51	6%	0.7188
5	KEGG RAS SIGNALING PATHWAY	0.149	0.32	2.52	3%	0.6594
6	KEGG SYNAPTIC VESICLE CYCLE	0.141	0.30	3.02	0%	0.6594
7	KEGG PPAR SIGNALING PATHWAY	0.130	0.30	2.79	3%	0.7437
8	KEGG MAPK SIGNALING PATHWAY	0.123	0.27	2.71	2%	0.6594
9	KEGG CITRATE CYCLE TCA CYCLE	0.097	0.23	2.32	0%	0.6594
10	KEGG FATTY ACID DEGRADATION	0.073	0.29	0.70	4%	0.8541

Note. *Composite scores were used for ranking and do not represent independent inferential statistics.*

Supported findings

Autophagy in triple-negative breast cancer

Table 2
Per-disease pathway enrichment

Gene set	Phenotype	n	Coverage	Stouffer Z	Bootstrap 95% CI	Permutation p	FDR
KEGG AUTOPHAGY ANIMAL	tn brs	153	90%	−8.98	[−14.78, −3.09]	.0022	.022
KEGG ENDOCYTOSIS	tn brs	241	96%	−5.68	[−11.28, 0.02]	.0417	.2085
KEGG NEUROACTIVE LIGAND RECEPTOR INTERACTION	brs ca	255	69%	+ 3.50	[− 0.93, 7.78]	.2304	.8874
KEGG SYNAPTIC VESICLE CYCLE	tn brs	68	86%	+ 3.02	[− 2.20, 8.34]	.2815	.6594
KEGG PPAR SIGNALING PATHWAY	brs ca	67	88%	+ 2.79	[− 2.16, 7.54]	.3491	.8874
KEGG MAPK SIGNALING PATHWAY	tn brs	266	89%	+ 2.71	[− 2.19, 7.66]	.3294	.6594
KEGG RAS SIGNALING PATHWAY	tn brs	209	88%	−2.52	[− 7.05, 1.89]	.3659	.6594
KEGG REGULATION OF ACTIN CYTOSKELETON	brs ca	192	83%	−2.51	[− 7.99, 2.93]	.3940	.8874
KEGG CITRATE CYCLE TCA CYCLE	tn brs	27	90%	+ 2.32	[− 3.02, 7.70]	.3957	.6594
KEGG CITRATE CYCLE TCA CYCLE	brs ca	26	87%	+ 2.17	[− 4.00, 8.12]	.4476	.6594
KEGG AUTOPHAGY ANIMAL	brs ca	—	—	+ 0.83	—	.7702	—
KEGG ENDOCYTOSIS	brs ca	—	—	−0.90	—	.7633	—
KEGG FATTY ACID DEGRADATION	brs ca	—	—	−0.70	—	.8051	—
KEGG FATTY ACID DEGRADATION	tn brs	—	—	−0.49	—	.8541	—

Note. brs ca = overall breast cancer; tn brs = triple-negative breast cancer.

Autophagy was the only pathway with convincing evidence across the principal enrichment and differential analyses. In TNBC, 153 of 169 pathway genes were available, giving 90% coverage. The robust pathway Stouffer Z was − 8.98, with a bootstrap 95% confidence interval of − 14.78 to − 3.09. The random-gene permutation p value was .0022, the pathway FDR across the ten tested sets was .022, and the Wilcoxon p value was .00074. By comparison, the corresponding overall breast cancer result was modest and non-significant: Z = + 0.83 and permutation p = .7702. The principal pathway enrichment results are summarized in Table 2.

The net negative TNBC score indicates a shift toward negative predicted-expression associations across the autophagy set. Subject to correct TWAS orientation, this is compatible with higher genetically predicted expression of the contributing genes being associated, on average, with lower TNBC susceptibility. The result does not show that autophagy is transcriptionally or functionally suppressed within established TNBC tumors.

The distribution of autophagy gene Z scores differed between overall breast cancer and TNBC. Among 143 genes scored in both datasets, the mean overall breast cancer minus TNBC difference was + 0.760. In the combined pairwise analysis, the Mann–Whitney global FDR was .0164, the Kolmogorov–Smirnov global FDR was .0105, and the Brunner–Munzel global FDR was .0158. The paired Wilcoxon p value was .0133. Effect sizes were small, however, with paired Cohen's d of approximately 0.15, unpaired Cohen's d of 0.25, and a rank-biserial correlation of about − 0.22. The evidence therefore points to a broad but modest distributional shift rather than uniformly large effects at individual genes.

The gene-level profiles were negatively correlated across the phenotypes. Pearson r was − 0.364 with p = .000008, Spearman rho was − 0.359 with p = .00001, and cosine similarity was − 0.355. These values indicate that genes with relatively positive scores in one analysis often had relatively negative scores in the other. Because the two GWAS datasets overlap and pathway genes are correlated, the nominal correlation p values cannot be treated as a formal case-case test.

Table 3
Tissue-level pathway enrichment highlights

Gene set	Tissue	brs ca Z	tn brs Z	Gap, brs ca − tn brs
KEGG AUTOPHAGY ANIMAL	Whole blood	+ 3.47	−2.52	+ 5.98
KEGG AUTOPHAGY ANIMAL	Liver	+ 1.96	−3.80	+ 5.76
KEGG AUTOPHAGY ANIMAL	Uterus	+ 2.40	−3.24	+ 5.63
KEGG AUTOPHAGY ANIMAL	EBV-transformed lymphocytes	+ 2.12	−3.22	+ 5.34
KEGG AUTOPHAGY ANIMAL	Spleen	−0.26	−4.31	+ 4.05
KEGG AUTOPHAGY ANIMAL	Subcutaneous adipose	+ 0.56	−1.41	+ 1.97
KEGG ENDOCYTOSIS	Subcutaneous adipose	+ 0.24	−3.71	+ 3.95
KEGG ENDOCYTOSIS	Liver	+ 0.49	−3.21	+ 3.69
KEGG ENDOCYTOSIS	Visceral omental adipose	−0.41	−3.57	+ 3.15
KEGG ENDOCYTOSIS	Breast mammary tissue	+ 0.55	−2.08	+ 2.63
KEGG ENDOCYTOSIS	Uterus	−0.57	−2.85	+ 2.28
KEGG ENDOCYTOSIS	Vagina	−0.62	−2.09	+ 1.47
KEGG NEUROACTIVE LIGAND RECEPTOR INTERACTION	Subcutaneous adipose	+ 3.15	−0.80	+ 3.95
KEGG NEUROACTIVE LIGAND RECEPTOR INTERACTION	Vagina	+ 1.88	−1.23	+ 3.11
KEGG NEUROACTIVE LIGAND RECEPTOR INTERACTION	Cultured fibroblasts	+ 2.58	+ 0.03	+ 2.55
KEGG NEUROACTIVE LIGAND RECEPTOR INTERACTION	Breast mammary tissue	+ 0.96	−1.48	+ 2.44
KEGG NEUROACTIVE LIGAND RECEPTOR INTERACTION	Visceral omental adipose	+ 1.51	−0.61	+ 2.11
KEGG NEUROACTIVE LIGAND RECEPTOR INTERACTION	Ovary	+ 0.76	−1.06	+ 1.82
KEGG REGULATION OF ACTIN CYTOSKELETON	EBV-transformed lymphocytes	−1.47	+ 3.07	−4.54
KEGG REGULATION OF ACTIN CYTOSKELETON	Spleen	−1.53	+ 1.82	−3.35

Gene set	Tissue	brs ca Z	tn brs Z	Gap, brs ca − tn brs
KEGG REGULATION OF ACTIN CYTOSKELETON	Breast mammary tissue	−1.90	+ 0.82	−2.72
KEGG REGULATION OF ACTIN CYTOSKELETON	Subcutaneous adipose	−2.40	+ 0.08	−2.48
KEGG REGULATION OF ACTIN CYTOSKELETON	Cultured fibroblasts	−2.21	+ 0.16	−2.37
KEGG REGULATION OF ACTIN CYTOSKELETON	Ovary	−0.58	+ 1.02	−1.60
KEGG RAS SIGNALING PATHWAY	Vagina	−0.04	−4.09	+ 4.05
KEGG RAS SIGNALING PATHWAY	Cultured fibroblasts	−3.64	−0.06	−3.58
KEGG RAS SIGNALING PATHWAY	Spleen	−2.82	+ 0.55	−3.38
KEGG RAS SIGNALING PATHWAY	Liver	+ 1.53	−1.41	+ 2.93
KEGG RAS SIGNALING PATHWAY	Breast mammary tissue	+ 0.12	−1.93	+ 2.04
KEGG RAS SIGNALING PATHWAY	Ovary	−1.03	+ 0.67	−1.70

The tissue results were directionally consistent. The mean overall breast cancer minus TNBC pathway gap was + 2.83 across the 11 tissues, with the same gap direction in 82% of them. TNBC autophagy Z scores were below − 1.96 in 82% of the tissues. The largest gaps occurred in whole blood, where the overall breast cancer and TNBC values were + 3.47 and − 2.52; liver, + 1.96 and − 3.80; uterus, + 2.40 and − 3.24; EBV-transformed lymphocytes, + 2.12 and − 3.22; and spleen, − 0.26 and − 4.31. These results are descriptive because tissue-level permutations were not performed and the models share both eQTL structure and the same GWAS outcome data. Tissue-level pathway gaps are shown in Table 3.

The raw, non-winsorized autophagy statistic was − 8.77 in the sensitivity analysis. No TNBC autophagy gene crossed the prespecified leave-one-out threshold, so no gene was removed and the statistic remained − 8.77. This is consistent with a distributed signal under the selected rule, but it is not a fully independent robustness test because the rule itself identified no exclusions.

MAP2K2 as a recurrent pathway bridge

MAP2K2 was the most direct individual connection between the breast cancer results and the NMN-responsive gene list. Across the complete influence output it appeared in four KEGG sets. Among the five highest-ranked divergent pathways, it was recurrent in autophagy, Ras signaling, and regulation of the actin cytoskeleton. Its cross-tissue gene-level score was approximately − 3.35 in overall breast cancer and + 6.08 in TNBC.

This opposite signed pattern is notable because MAP2K2 was also reported as a directionally consistent NMN-responsive gene in liver and white adipose tissue [8]. In the breast cancer analysis, however, the repeated MAP2K2 result was not independent across pathways. The same gene-level TWAS value was counted wherever MAP2K2 appeared in an overlapping KEGG set.

The findings nominate MAP2K2 for gene-centered analysis but do not establish that its predicted expression causes TNBC. No locus-level colocalization, conditional TWAS, or gene-wide multiple-testing result was available. The appropriate interpretation is that MAP2K2 had a marked subtype-opposed TWAS pattern within several related pathways and merits investigation as a possible regulatory contributor.

Suggestive findings

Endocytosis and the RAB11A hypothesis

Endocytosis produced the second-largest TNBC pathway statistic. Among 250 pathway members, 241 were available. The robust Stouffer Z was − 5.68, with a bootstrap confidence interval of − 11.28 to + 0.02. The permutation p value was .0417, but the pathway FDR was .2085, and the Wilcoxon p value was .0646. The interval crossed zero and the competitive result did not survive correction. Endocytosis was therefore suggestive rather than supported at the same level as autophagy.

The overall breast cancer–TNBC profile correlation was negative, with Pearson r = − 0.331 and Spearman rho = − 0.335. The mean tissue gap was + 1.53, and 73% of tissues had the same gap direction. TNBC endocytosis scores were below − 1.96 in 64% of tissues, with prominent differences in subcutaneous adipose, liver, visceral adipose, breast mammary tissue, and uterus.

RAB11A provided the reason for selecting endocytosis as an NMN-linked pathway. RAB11A-positive recycling endosomes contribute membrane and organizational platforms for autophagosome assembly and regulate receptor recycling [18, 19]. Receptor recycling can also alter the duration of growth-factor signaling, including EGFR-related pathways [20]. RAB11A itself was not among the major leave-one-out drivers in the current endocytosis output. The pathway result therefore cannot be used as direct evidence that RAB11A is a breast cancer susceptibility gene.

Fatty-acid degradation and CPT2

Fatty-acid degradation was not enriched in either phenotype. The overall breast cancer result was Z = − 0.70 with permutation p = .8051, and the TNBC result was Z = − 0.49 with permutation p = .8541. Despite the lack of collective enrichment, the profiles were strongly anticorrelated. Pearson r was − 0.448, Spearman rho was − 0.533, and Kendall tau was − 0.377. The Kendall p value was .000614, with a test-specific global FDR of approximately .00077.

CPT2 had a modest negative score in overall breast cancer, approximately − 1.39, and a positive TNBC score of approximately + 2.61. CPT2 is located on the inner mitochondrial membrane and supports long-

chain fatty-acid oxidation through the carnitine shuttle [21]. The observed pattern is consistent with directional heterogeneity in the fatty-acid pathway, not evidence that the pathway is collectively enriched or that CPT2 has a causal effect on TNBC.

Other fatty-acid genes had large and sometimes opposing scores, including ACAT1, ACAA1, ECI1, ACOX3, HADH, and several alcohol and aldehyde dehydrogenases. This mixture helps explain why pathway correlation detected subtype divergence while the net pathway enrichment remained close to zero.

Other pathway results and sensitivity findings

Table 4
Between-phenotype differential, profile, and classification results

Gene set	Analysis or classification	Estimate	p value	FDR	Interpretation
KEGG AUTOPHAGY ANIMAL	Mann–Whitney differential test	Mean difference = + 0.760	.001546	.001546	Different distributions
KEGG AUTOPHAGY ANIMAL	Paired Wilcoxon	—	.013337	.019493	Paired shift
KEGG AUTOPHAGY ANIMAL	Kolmogorov–Smirnov	—	.001049	.003116	Distributional difference
KEGG AUTOPHAGY ANIMAL	Brunner–Munzel	—	.001579	.003116	Distributional difference
KEGG AUTOPHAGY ANIMAL	Paired Cohen's d	+ 0.15	—	—	Small effect
KEGG AUTOPHAGY ANIMAL	Unpaired Cohen's d	+ 0.25	—	—	Small effect
KEGG AUTOPHAGY ANIMAL	Rank-biserial correlation	−0.217	—	—	Small effect
KEGG AUTOPHAGY ANIMAL	Pearson profile correlation	r = − 0.364	.000008	—	Opposite profile ordering
KEGG AUTOPHAGY ANIMAL	Spearman profile correlation	ρ = −0.359	.000010	—	Opposite rank ordering
KEGG ENDOCYTOSIS	Pearson / Spearman	r = − .331; ρ = −.335	< .001	< .001	Discordant profiles
KEGG NEUROACTIVE LIGAND RECEPTOR INTERACTION	Pearson / Spearman	r = − .385; ρ = −.389	< .001	< .001	Discordant profiles
KEGG RAS SIGNALING PATHWAY	Spearman	ρ = −.325	.000003	.0000285	Rank discordance
KEGG SYNAPTIC VESICLE CYCLE	Pearson / Spearman	r = − .385; ρ = −.426	.001694 / .000450	.010729 / .005045	Discordant profiles

Gene set	Analysis or classification	Estimate	p value	FDR	Interpretation
KEGG FATTY ACID DEGRADATION	Pearson / Spearman	r = − .448; ρ = −.533	.003740 / .000401	.023687 / .005833	Strong discordance
KEGG PPAR SIGNALING PATHWAY	Pearson / Spearman	r = − .309; ρ = −.308	.010860 / .011260	—	Moderate discordance
Shared, same direction	KEGG CITRATE CYCLE TCA CYCLE	brs ca Z = + 2.17; tn brs Z = + 2.32	—	—	Shared pathway pattern
Specific to brs ca	KEGG NEUROACTIVE LIGAND RECEPTOR INTERACTION	brs ca Z = + 3.50; tn brs Z = + 1.20	—	—	Stronger in overall breast cancer
Specific to brs ca	KEGG PPAR SIGNALING PATHWAY	brs ca Z = + 2.79; tn brs Z = + 1.13	—	—	Stronger in overall breast cancer
Specific to brs ca	KEGG REGULATION OF ACTIN CYTOSKELETON	brs ca Z = − 2.51; tn brs Z = + 1.82	—	—	Directionally divergent
Specific to tn brs	KEGG AUTOPHAGY ANIMAL	brs ca Z = + 0.83; tn brs Z = − 8.98	—	—	TNBC-specific enrichment
Specific to tn brs	KEGG ENDOCYTOSIS	brs ca Z = − 0.90; tn brs Z = − 5.68	—	—	TNBC-specific enrichment
Specific to tn brs	KEGG SYNAPTIC VESICLE CYCLE	brs ca Z = + 1.76; tn brs Z = + 3.02	—	—	Stronger in TNBC
Specific to tn brs	KEGG MAPK SIGNALING PATHWAY	brs ca Z = − 1.42; tn brs Z = + 2.71	—	—	Directionally divergent
Specific to tn brs	KEGG RAS SIGNALING PATHWAY	brs ca Z = − 0.43; tn brs Z = − 2.52	—	—	Stronger in TNBC

Several pathways crossed an absolute Stouffer threshold without competitive evidence of enrichment. In overall breast cancer, neuroactive ligand–receptor interaction had Z = + 3.50 but permutation p = .2304; PPAR signaling had Z = + 2.79 and p = .3491; regulation of the actin cytoskeleton had Z = − 2.51 and p = .3940; and the citrate cycle had Z = + 2.17 and p = .4476. Their bootstrap intervals crossed zero. These results were exploratory and should not be described as statistically supported enrichment.

The same issue applied to several TNBC pathways. The synaptic vesicle cycle had Z = + 3.02 and permutation p = .2815; MAPK signaling had Z = + 2.71 and p = .3294; Ras signaling had Z = − 2.52 and p = .3659; and the citrate cycle had Z = + 2.32 and p = .3957.

The influence-removal analysis classified seven pathway–phenotype combinations as stable at an absolute Z threshold of 1.96. These were TNBC autophagy and endocytosis; overall breast cancer neuroactive ligand–receptor interaction, actin regulation, PPAR signaling, and the citrate cycle; and the TNBC synaptic vesicle cycle. Four results lost the threshold after flagged genes were removed: the TNBC citrate cycle changed from + 2.38 to + 1.29, TNBC MAPK signaling from + 2.00 to + 0.84, the overall breast cancer synaptic vesicle cycle from + 2.00 to + 0.76, and TNBC actin regulation from + 1.97 to + 0.26. Except for TNBC autophagy, threshold stability did not imply permutation or FDR significance. The differential and profile analyses are summarized in Table 4.

Gene-level leads

The relative leave-one-out rule flagged 726 gene–phenotype entries, including 96 sign reversals. The largest counts occurred in neuroactive ligand–receptor interaction, autophagy, and endocytosis, with 225, 136, and 84 flagged entries, respectively. Many arose when the full pathway score was close to zero, making a small absolute change appear large in percentage terms. These counts should not be viewed as 726 independent associations.

HRAS was recurrent in five complete pathway sets and in four of the five highest-ranked divergent pathways. Other recurring genes included FGFR2, AKT1, MAP2K1, MAPK9, MAPK10, CDC42, FGFR4, PRKACB, PDGFD, and several PI3K components. Their recurrence largely reflected shared membership in connected signaling pathways.

TP53INP2 had an overall breast cancer Z of approximately − 5.53 within the autophagy set. TP53INP2 is required for mammalian autophagy and contributes to autophagosome formation through interactions involving LC3 and ATG7 [22, 23]. The result was not corrected as a gene-level discovery, and a corresponding TNBC-specific causal mechanism was not established.

GALR1 had a TNBC score of approximately + 2.96 within the neuroactive ligand–receptor pathway. CPT2 had the subtype-opposed pattern described above. RAB11A did not emerge as a major pathway driver. These genes remain candidates for focused follow-up rather than validated susceptibility genes.

The pooled global BH analysis yielded 38 entries below .05, many involving repeated correlation, Kendall, sign-concordance, and differential tests applied to the same pathway. These entries supported the general pattern of subtype divergence but did not constitute 38 independent findings. The sensitivity and influential-gene summaries are presented in Table 5, and the pooled FDR survivors are listed in Table 6.

Table 5
Sensitivity and gene-level influence results Panel A. Sensitivity analysis after removal of influential genes

Phenotype	Gene set	Full Z	Z without influential genes	Genes dropped	Interpretation
tn brs	KEGG AUTOPHAGY ANIMAL	−8.77	−8.77	0	Robust
tn brs	KEGG ENDOCYTOSIS	−5.24	−5.24	0	Robust
brs ca	KEGG NEUROACTIVE LIGAND RECEPTOR INTERACTION	+ 4.11	+ 3.17	1	Robust
tn brs	KEGG SYNAPTIC VESICLE CYCLE	+ 3.59	+ 3.91	3	Robust
brs ca	KEGG REGULATION OF ACTIN CYTOSKELETON	−2.87	−2.45	4	Robust
brs ca	KEGG PPAR SIGNALING PATHWAY	+ 2.76	+ 2.58	7	Robust
brs ca	KEGG CITRATE CYCLE TCA CYCLE	+ 2.16	+ 2.02	9	Robust
tn brs	KEGG CITRATE CYCLE TCA CYCLE	+ 2.38	+ 1.29	12	Fragile
tn brs	KEGG MAPK SIGNALING PATHWAY	+ 2.00	+ 0.84	6	Fragile
brs ca	KEGG SYNAPTIC VESICLE CYCLE	+ 2.00	+ 0.76	16	Fragile
tn brs	KEGG REGULATION OF ACTIN CYTOSKELETON	+ 1.97	+ 0.26	13	Fragile

Panel B. Recurrent influential genes across top divergent pathways

Gene	Number of pathways	Maximum relative change in Z	Pathways
HRAS	4	675.94%	Autophagy; endocytosis; Ras signaling; regulation of actin cytoskeleton
MAP2K2	3	258.31%	Autophagy; Ras signaling; regulation of actin cytoskeleton
FGFR2	3	76.72%	Endocytosis; Ras signaling; regulation of actin cytoskeleton
PIK3R3	2	596.42%	Autophagy; Ras signaling
MAPK10	2	518.14%	Autophagy; Ras signaling
MAP2K1	2	472.29%	Autophagy; Ras signaling
PIK3CB	2	362.60%	Autophagy; Ras signaling
PIK3CD	2	298.31%	Autophagy; Ras signaling
PIK3R2	2	246.24%	Autophagy; Ras signaling
AKT1	2	206.01%	Autophagy; Ras signaling
PIK3R1	2	193.60%	Autophagy; Ras signaling
PIK3CA	2	189.16%	Autophagy; Ras signaling
BAD	2	188.59%	Autophagy; Ras signaling
MAPK9	2	185.64%	Autophagy; Ras signaling
CDC42	2	62.95%	Endocytosis; Ras signaling
FGFR4	2	62.80%	Endocytosis; Ras signaling
ARPC5	2	61.61%	Endocytosis; regulation of actin cytoskeleton
ACTR3	2	53.41%	Endocytosis; regulation of actin cytoskeleton
PDGFD	2	48.47%	Ras signaling; regulation of actin cytoskeleton
PLD2	2	44.54%	Endocytosis; Ras signaling
PRKACB	2	40.87%	Autophagy; Ras signaling
RHOA	2	35.59%	Endocytosis; Ras signaling
RAB5C	2	32.56%	Endocytosis; Ras signaling
ARF6	2	30.18%	Endocytosis; Ras signaling

Panel C. Highest-impact leave-one-out genes

Gene set and phenotype	Gene	Gene Z	Δ Stouffer Z	Relative change	Sign flip
Neuroactive ligand–receptor; tn brs	POMC	−28.31	−1.73	1648.7%	No
Autophagy; brs ca	ATG10	−20.91	−1.75	1612.3%	No
Autophagy; brs ca	VPS11	+ 11.11	+ 0.93	856.1%	Yes
Autophagy; brs ca	WDR45B	−10.76	−0.90	830.2%	No
Autophagy; brs ca	BECN1	+ 10.05	+ 0.84	774.4%	Yes
Neuroactive ligand–receptor; tn brs	CHRNG	+ 13.20	+ 0.81	768.7%	Yes
Autophagy; brs ca	HRAS	−8.76	−0.74	675.9%	No
Autophagy; brs ca	CFLAR	−8.19	−0.69	631.8%	No
Autophagy; brs ca	PIK3R3	−7.73	−0.65	596.4%	No
Autophagy; brs ca	GABARAP	+ 7.46	+ 0.63	574.6%	Yes
Autophagy; brs ca	ATG13	−7.37	−0.62	568.4%	No
Neuroactive ligand–receptor; tn brs	UTS2R	+ 9.74	+ 0.59	567.1%	Yes
Neuroactive ligand–receptor; tn brs	QRFP	+ 8.99	+ 0.55	523.3%	Yes
Autophagy; brs ca	MAPK10	−6.72	−0.56	518.1%	No
Autophagy; brs ca	VMP1	+ 6.52	+ 0.55	502.5%	Yes
Neuroactive ligand–receptor; tn brs	AGT	+ 8.59	+ 0.52	500.2%	Yes
Autophagy; brs ca	MAP2K1	−6.12	−0.51	472.3%	No
Neuroactive ligand–receptor; tn brs	LTB4R2	+ 7.96	+ 0.49	463.6%	Yes
Autophagy; brs ca	GORASP2	+ 5.94	+ 0.50	457.6%	Yes
Autophagy; brs ca	GORASP1	−5.89	−0.49	454.6%	No

Note. Robust results were significant before and after removal of influential genes. Fragile results lost the |Z| > 1.96 threshold after removal and should be interpreted cautiously. Relative leave-one-out influence does not establish independent genetic causality.

Table 6
Pooled family-wise FDR survivors

Gene set	Source	Test	Comparison	p	FDR
KEGG ENDOCYTOSIS	Proximity	Spearman	brs ca vs tn brs	0	0
KEGG ENDOCYTOSIS	Proximity	Pearson	brs ca vs tn brs	0	0
KEGG ENDOCYTOSIS	Pairwise	Kendall	brs ca vs tn brs	0	0
KEGG NEUROACTIVE LIGAND RECEPTOR INTERACTION	Proximity	Pearson	brs ca vs tn brs	0	0
KEGG NEUROACTIVE LIGAND RECEPTOR INTERACTION	Proximity	Spearman	brs ca vs tn brs	0	0
KEGG NEUROACTIVE LIGAND RECEPTOR INTERACTION	Pairwise	Kendall	brs ca vs tn brs	0	0
KEGG RAS SIGNALING PATHWAY	Proximity	Spearman	brs ca vs tn brs	3×10^{-6}	2.85×10^{-5}
KEGG RAS SIGNALING PATHWAY	Pairwise	Kendall	brs ca vs tn brs	3×10^{-6}	2.85×10^{-5}
KEGG AUTOPHAGY ANIMAL	Proximity	Pearson	brs ca vs tn brs	8×10^{-6}	6.33×10^{-5}
KEGG AUTOPHAGY ANIMAL	Pairwise	Kendall	brs ca vs tn brs	9×10^{-6}	6.33×10^{-5}
KEGG AUTOPHAGY ANIMAL	Proximity	Spearman	brs ca vs tn brs	1×10^{-5}	6.33×10^{-5}
KEGG MAPK SIGNALING PATHWAY	Proximity	Spearman	brs ca vs tn brs	3×10^{-5}	3.23×10^{-4}
KEGG MAPK SIGNALING PATHWAY	Pairwise	Kendall	brs ca vs tn brs	3.4×10^{-5}	3.23×10^{-4}
KEGG REGULATION OF ACTIN CYTOSKELETON	Pairwise	Kendall	brs ca vs tn brs	2.2×10^{-5}	3.33×10^{-4}
KEGG REGULATION OF ACTIN CYTOSKELETON	Proximity	Spearman	brs ca vs tn brs	3.5×10^{-5}	3.33×10^{-4}

Note. The pooled output was labeled "family-wise FDR" by the pipeline, but it represents a pooled global Benjamini–Hochberg adjustment across correlated and partly duplicated tests. It should not be interpreted as control of the family-wise error rate or as 38 independent discoveries.

Gene set	Source	Test	Comparison	p	FDR
KEGG NEUROACTIVE LIGAND RECEPTOR INTERACTION	Pairwise	Sign concordance	brs ca vs tn brs	7.1 × 10 − 5	3.37 × 10 − 4
KEGG REGULATION OF ACTIN CYTOSKELETON	Proximity	Pearson	brs ca vs tn brs	9.2 × 10 − 5	5.83 × 10 − 4
KEGG REGULATION OF ACTIN CYTOSKELETON	Pairwise	Sign concordance	brs ca vs tn brs	.000379	.001800
KEGG ENDOCYTOSIS	Pairwise	Sign concordance	brs ca vs tn brs	.000529	.002513
KEGG AUTOPHAGY ANIMAL	Pairwise	Sign concordance	brs ca vs tn brs	.000534	.002536
KEGG AUTOPHAGY ANIMAL	Enrichment	Wilcoxon	tn brs	.000740	.002812
KEGG AUTOPHAGY ANIMAL	Pairwise	KS	brs ca vs tn brs	.001049	.003116
KEGG AUTOPHAGY ANIMAL	Differential	Kruskal–Wallis	All diseases	.001542	.003116
KEGG AUTOPHAGY ANIMAL	Differential	Mann–Whitney U	brs ca vs tn brs	.001546	.003116
KEGG AUTOPHAGY ANIMAL	Pairwise	Brunner–Munzel	brs ca vs tn brs	.001579	.003116
KEGG AUTOPHAGY ANIMAL	Pairwise	Mann–Whitney U	brs ca vs tn brs	.001640	.003116
KEGG RAS SIGNALING PATHWAY	Proximity	Pearson	brs ca vs tn brs	.000584	.003699
KEGG AUTOPHAGY ANIMAL	Enrichment	Permutation	tn brs	.002200	.003800
KEGG SYNAPTIC VESICLE CYCLE	Proximity	Spearman	brs ca vs tn brs	.000450	.005045
KEGG SYNAPTIC VESICLE CYCLE	Pairwise	Kendall	brs ca vs tn brs	.000531	.005045
KEGG FATTY ACID DEGRADATION	Proximity	Spearman	brs ca vs tn brs	.000401	.005833
KEGG FATTY ACID DEGRADATION	Pairwise	Kendall	brs ca vs tn brs	.000614	.005833

Note. The pooled output was labeled “family-wise FDR” by the pipeline, but it represents a pooled global Benjamini–Hochberg adjustment across correlated and partly duplicated tests. It should not be interpreted as control of the family-wise error rate or as 38 independent discoveries.

Gene set	Source	Test	Comparison	p	FDR
KEGG SYNAPTIC VESICLE CYCLE	Proximity	Pearson	brs ca vs tn brs	.001694	.010729
KEGG AUTOPHAGY ANIMAL	Pairwise	Paired Wilcoxon	brs ca vs tn brs	.013337	.019493
KEGG AUTOPHAGY ANIMAL	Differential	Paired Wilcoxon	brs ca vs tn brs	.013337	.019493
KEGG FATTY ACID DEGRADATION	Proximity	Pearson	brs ca vs tn brs	.003740	.023687
KEGG RAS SIGNALING PATHWAY	Pairwise	Sign concordance	brs ca vs tn brs	.005209	.024743
KEGG AUTOPHAGY ANIMAL	Pairwise	Welch	brs ca vs tn brs	.035183	.047748

Note. The pooled output was labeled "family-wise FDR" by the pipeline, but it represents a pooled global Benjamini–Hochberg adjustment across correlated and partly duplicated tests. It should not be interpreted as control of the family-wise error rate or as 38 independent discoveries.

Discussion

Mechanistic synthesis

The central result was a strong negative signed autophagy association in TNBC (Fig. 2). Its importance rests on the agreement among several features: high pathway coverage, a permutation result that survived correction across the ten pathways, a confidence interval that excluded zero, a significant shift from the overall breast cancer gene distribution, and a similar overall–TNBC gap across most tissues. No other pathway met the same combination of criteria.

Autophagy offers a biologically plausible connection to susceptibility because it protects normal cells from several forms of damage associated with tumor initiation. By removing dysfunctional mitochondria, protein aggregates, and other damaged components, basal autophagy can limit reactive oxygen species, chronic inflammatory signaling, and genome instability. Experimental loss of autophagy has been linked to p62 accumulation, altered stress responses, chromosomal instability, and tumor development in model systems [24, 12]. In breast models, reduced autophagy has also been associated with genomic damage and tumorigenic changes [32].

Under this model, inherited expression patterns that modestly reduce the maintenance capacity of autophagy-related systems could contribute to TNBC vulnerability before a tumor forms. This interpretation is compatible with the net negative TWAS score, provided the prediction models and alleles were correctly oriented. It remains a hypothesis, however. The pathway statistic combines genes with different functions and directions, and predicted expression is not a direct measure of autophagic activity.

The same pathway may have a different role after malignant transformation. Established tumors can use autophagy to obtain metabolic substrates, maintain mitochondrial function, survive hypoxia, and resist treatment. Some breast cancer and TNBC models depend on autophagy for proliferation, migration, stem-like properties, or chemotherapy tolerance [25, 26, 14]. Autophagy inhibition has therefore been proposed for selected established cancers, while intact basal autophagy may protect normal tissues from tumor initiation [11, 27].

This stage-dependent biology prevents a simple therapeutic conclusion. A germline pattern compatible with reduced susceptibility at higher predicted expression does not mean that autophagy should be stimulated in an existing TNBC. Conversely, evidence that some tumors rely on autophagy does not invalidate a possible protective role before tumor initiation. Prevention, tumor maintenance, treatment response, and host metabolism represent different biological settings.

MAP2K2 provides a second line of interpretation. It encodes MEK2, one of the kinases linking RAS and RAF to ERK1/2. This pathway regulates growth, survival, stress adaptation, cytoskeletal organization, and aspects of autophagy. RAS–RAF–MEK–ERK signaling has long been considered a possible dependency in molecular subsets of TNBC, although pathway activation does not consistently predict response to MEK inhibition [28, 29].

The negative overall breast cancer and positive TNBC MAP2K2 scores are consistent with subtype-specific regulatory effects. They should not be described as proof that MAP2K2 is protective in one phenotype and causal in the other. The overall analysis includes TNBC cases, the two GWAS datasets are correlated, and the TWAS signal could reflect linkage disequilibrium with another gene or variant. The result is best used to justify colocalization and functional studies.

MAP2K2 also illustrates the difference between recurrence and replication. Its appearance in autophagy, Ras, MAPK, and cytoskeletal pathways reflects real biological connectivity, but these observations use the same gene score more than once. The finding gains relevance because MAP2K2 was independently nominated by the NMN-responsive gene analysis, not because its appearance in overlapping KEGG pathways constitutes several independent genetic associations.

The tissue pattern adds another layer but should be interpreted carefully. Liver, adipose tissue, spleen, blood, uterus, and cultured cells showed prominent autophagy gaps. These tissues participate in metabolic and immune regulation, making a systemic stress-response interpretation plausible. Their direction also resembles the tissue-specific character of the NMN transcriptional response described by Cheung [8], in which no robust gene was rescued in all three metabolic tissues.

Nevertheless, a liver or blood S-PrediXcan association does not prove that liver or blood mediates TNBC risk. Prediction models in different tissues often share eQTLs, and all tissue tests used the same GWAS outcomes. The broad pattern may reflect shared cis-regulation that is detectable through several tissues rather than separate organ-level mechanisms.

Convergence with NMN-responsive aging biology

The overlap between the two studies is best described as cross-context pathway convergence. The NMN analysis began with expression responses in normal metabolic tissues from aged mice. The breast cancer analysis began with human germline variants and expression-prediction models. These are different species, experimental designs, tissues, and outcomes.

Within that constraint, the convergence is coherent. The NMN-derived framework nominated RAB11A and endosomal recycling, CPT2 and fatty-acid oxidation, MAP2K2 and Ras/MAPK signaling, and TP53INP2-related autophagy. The present analysis identified autophagy as its clearest TNBC pathway, MAP2K2 as its strongest recurrent nominated gene, endocytosis as a suggestive pathway, and fatty-acid degradation as a source of subtype-opposed gene patterns.

NAD-positive biology provides a possible connection among these systems. SIRT1 can regulate autophagy proteins, while AMPK and mTOR control ULK1-dependent autophagy initiation [6, 7]. NMN exposure has also been linked to SIRT1–AMPK signaling in adipocyte models [30]. These findings support biological plausibility but do not establish a single NMN-to-autophagy mechanism in breast tissue or cancer.

No result from this study shows that NMN lowers or raises breast cancer risk. The original long-term experiment examined physiological aging in mice, and the Cheung analysis was an underpowered, hypothesis-generating reanalysis reported as a preprint. Any proposal to use NMN or another NAD-positive precursor in people at risk of TNBC would require dedicated toxicology, prevention, pharmacology, and tumor-context studies.

Subtype heterogeneity

The negative gene-profile correlations are compatible with the subtype heterogeneity described in the source GWAS. Zhang et al. [2] found loci with opposite effects across luminal and non-luminal disease and only partial genetic correlations among intrinsic-like subtypes. The present results extend that observation to predicted-expression profiles within selected biological pathways.

Autophagy, endocytosis, neuroactive signaling, fatty-acid degradation, the synaptic vesicle cycle, PPAR signaling, and Ras signaling all showed negative profile relationships under at least one correlation measure. Fatty-acid degradation was the clearest example of heterogeneity without enrichment. Its overall pathway score was close to zero in both phenotypes because positive and negative genes offset one another, yet the ordering and direction of those genes differed markedly between the analyses.

The prevalence of negative correlations also calls for technical checks. The effect alleles and S-PrediXcan model orientations should be verified across both GWAS datasets. A genome-wide correlation should be calculated using all genes available in both analyses. If the genome-wide relationship is also strongly negative, the pathway results may reflect a broader feature of the input data. If the genome-wide

relationship is positive or near zero while the nominated pathways remain negative, the evidence for pathway-specific heterogeneity would be stronger.

A direct case-case analysis would be preferable. Rather than comparing TNBC with a category that includes TNBC, a case-case GWAS can compare TNBC with non-TNBC breast cancer and model subtype-informative alleles explicitly. Recent case-case breast cancer analyses illustrate how this design can isolate variants related to subtype rather than general disease susceptibility [31].

Clinical and translational relevance

TNBC risk prediction remains less developed than risk prediction for some hormone receptor-positive forms of breast cancer. The current findings suggest that autophagy-related germline regulation could be evaluated as one component of subtype-focused stratification. A pathway score derived from validated autophagy eQTLs might eventually help distinguish individuals more likely to develop TNBC rather than another subtype. Such a score is not ready for clinical use. It would first need to predict subtype in independent cohorts, add information beyond established breast cancer polygenic scores, and perform consistently across ancestral groups.

MAP2K2 may offer a narrower biomarker hypothesis. If its locus colocalizes with both expression and TNBC susceptibility, genetically predicted MAP2K2 regulation could be tested for association with tumor features or treatment response. The present results do not show that inherited MAP2K2 expression predicts sensitivity to MEK inhibition. Trametinib and related agents inhibit MEK1 and MEK2 rather than acting as MEK2-specific drugs. Pharmacological experiments should therefore be described as MEK1/2 inhibition unless gene-specific perturbation is used.

Autophagy-related tumor biomarkers also require care. LC3, p62, autophagosome number, and expression of autophagy genes do not individually establish autophagic flux. Tumors may accumulate autophagosomes because autophagy is induced or because lysosomal completion is blocked. Functional assays that measure flux under controlled conditions are more informative than static expression measurements [11].

The endocytosis finding supports a related trafficking hypothesis. RAB11A-positive compartments participate in recycling and autophagosome formation, while recycling endosomes can restrain or sustain signaling depending on cargo and cellular context [18, 19]. If a RAB11A locus shows direct TNBC colocalization, the relevant consequences could include altered receptor recycling, nutrient-transporter localization, or autophagosome assembly. At present, the pathway association is not sufficient to assign any of these mechanisms to human susceptibility.

CPT2 and fatty-acid oxidation offer another testable direction. TNBC metabolism is heterogeneous: some tumors are mainly glycolytic, while others retain substantial oxidative or lipid-dependent metabolism [32, 33]. The CPT2 result may indicate that inherited regulation of substrate use has

different consequences across breast cancer subtypes. It does not show that all TNBCs depend on fatty-acid oxidation or that CPT2 inhibition would be beneficial.

Priorities for validation

The first priority is gene-level colocalization. MAP2K2, TP53INP2, RAB11A, and CPT2 should be tested to determine whether the same local variant is responsible for both the eQTL and breast cancer association. Methods that account for several causal variants are preferable because breast cancer loci and expression traits can show allelic heterogeneity. Conditional TWAS should then assess whether each candidate remains associated after neighboring predicted-expression signals are included [17].

Fine-mapping should be performed separately for overall breast cancer and TNBC, followed by a covariance-aware or case-case comparison. This is particularly important for MAP2K2 because its opposite scores are a major part of its appeal. If the positive TNBC and negative overall signals arise from different linked variants, the biological interpretation would differ from a single regulatory variant with subtype-dependent effects.

Functional work should begin with gene-specific perturbation rather than broad drug treatment. Candidate autophagy genes can be reduced or increased in several TNBC and luminal breast cancer models, followed by measurements of LC3 turnover, p62 degradation, lysosomal completion, mitochondrial quality, and survival during glucose deprivation or hypoxia. MDA-MB-231 and BT-549 are reasonable TNBC models, but no single cell line represents the full subtype.

MAP2K2 can be tested with CRISPR interference, knockout, or rescue constructs to separate MEK2-specific effects from combined MEK1/2 inhibition. Readouts should include ERK activity, autophagic flux, growth under metabolic stress, apoptosis, and changes in cytoskeletal behavior. The aim would not be to prove an NMN mechanism but to determine whether the subtype-opposed genetic signal corresponds to a measurable TNBC phenotype.

RAB11A experiments should examine recycling-endosome organization, EGFR or other receptor trafficking, nutrient-transporter localization, and autophagosome formation. CPT2 experiments should quantify fatty-acid oxidation, oxygen consumption, acylcarnitine accumulation, and survival during lipid-rich or glucose-limited conditions. These studies should include normal mammary epithelial cells and non-TNBC breast cancer models so that tumor-specific effects can be distinguished from general cellular stress.

The pathway findings should also be tested in independent human datasets. An autophagy-focused germline score could be evaluated in case-case cohorts, ideally comparing TNBC directly with hormone receptor-positive or HER2-positive disease. Analyses should be repeated in non-European ancestry populations because the Zhang et al. discovery resource was largely restricted to European ancestry. Replication should use prespecified pathways and avoid reselection based on the same NMN mapping.

Limitations

The main limitation is the distinction between pathway nomination and direct NMN-gene evidence. The tested gene sets were full KEGG pathways, often containing hundreds of genes. A significant autophagy result could be driven by pathway members that were not among the 35 NMN-responsive genes. The finding establishes pathway-level overlap, not direct enrichment of the original 35 genes. Separate analyses of all 35 genes, the 26 direction-consistent genes, and pathway intersections with the 35-gene set are needed.

The pathways were also selected after inspection of the NMN-derived genes. This is acceptable for hypothesis generation but narrows the interpretation of p values. The analysis did not represent an unbiased scan of all biological pathways.

The cross-tissue Stouffer procedure treated tissue models as approximately independent. GTEx tissues share eQTLs, and every tissue analysis used the same GWAS. Similarly, genes within a KEGG pathway can be correlated through linkage disequilibrium, shared predictors, genomic proximity, or common regulation. These dependencies can make nominal Stouffer statistics and bootstrap intervals too narrow. The random-gene permutation addressed pathway size but did not match genes for expression heritability, number of model SNPs, genomic clustering, or gene–gene correlation.

Some individual cross-tissue scores were extreme, including values with absolute Z greater than 20. These may reflect true strong associations, accumulation of correlated tissue evidence, or input and model features. Tissue-covariance-aware methods and gene-level quality control are needed before such scores are interpreted biologically.

The comparison between overall breast cancer and TNBC did not account directly for participant overlap or the fact that TNBC is included within overall breast cancer. Standard paired and unpaired tests applied to the gene Z vectors do not model GWAS sampling covariance. The differential p values should therefore be regarded as approximate.

The influence analysis also had important constraints. Percentage change becomes very large when the original pathway Z is near zero, explaining many of the 726 flagged entries and sign reversals. Conversely, a pathway with a large starting Z may have no genes exceed a 20% threshold even when individual absolute changes are meaningful. The unchanged TNBC autophagy sensitivity result is reassuring only within this prespecified definition.

The pooled global BH procedure did not control the probability of any false positive and should not be called a family-wise error correction. It combined correlated tests and, in some cases, repeated versions of the same underlying association. The 38 surviving entries were therefore not independent discoveries.

Finally, TWAS does not establish causality. A significant predicted-expression association can arise through linkage disequilibrium or pleiotropy, and the relevant tissue may not be the one in which the prediction model detected the signal. The Cheung study was a mouse reanalysis reported as a preprint,

and species-specific gene symbols, orthology, tissue composition, and experimental dose further limit direct translation.

Future directions

The most useful extension would combine TNBC-versus-non-TNBC case-case GWAS data with tissue-aware colocalization, conditional TWAS, and fine-mapping. Single-cell and spatial breast data could then show whether nominated genes are expressed in malignant epithelial cells, stromal cells, or immune populations and whether their expression corresponds to functional autophagy states.

Therapeutic studies should be restricted to biomarker-defined settings. Autophagy stimulation, autophagy inhibition, MEK1/2 inhibition, RAB11A perturbation, and fatty-acid oxidation targeting could each have different consequences depending on tumor stage and genotype. The present study supplies hypotheses for those experiments. It does not support NMN supplementation or generalized autophagy induction as a breast cancer prevention or treatment strategy.

Conclusion

This analysis found that the KEGG autophagy pathway had a strong negative signed TWAS association with TNBC susceptibility. The result survived competitive pathway correction, was observed across most available tissue models, and was not explained by a single gene under the prespecified influence rule. The corresponding overall breast cancer signal was weak, and the gene-level profiles differed between the two phenotypes, although their overlap prevents a definitive case-case interpretation.

MAP2K2 was the clearest individual bridge to the NMN-derived framework. Its opposite signed associations and recurrence across connected pathways justify colocalization and functional follow-up. Endocytosis and RAB11A remain suggestive, while CPT2 and fatty-acid degradation point to subtype heterogeneity rather than collective pathway enrichment.

The findings support a limited but testable conclusion: pathways nominated by NMN-responsive aging studies overlap with inherited TNBC susceptibility, most clearly at autophagy and MAP2K2. They neither establish the original 35 genes as causal nor show that NMN modifies breast cancer risk. Progress toward clinical application will require independent case-case validation, tissue-covariance-aware analysis, colocalization, and functional experiments in biomarker-defined models.

Declarations

Ethics approval and consent to participate

Not applicable. This study is a secondary analysis of publicly available genome-wide association study (GWAS) summary statistics and did not involve the collection of new human data or direct interaction with human participants.

Consent for publication

Not applicable.

Availability of data and materials

The overall breast cancer and triple-negative breast cancer GWAS summary statistics analyzed in this study were derived from Zhang et al. (2020) and are publicly available from the Breast Cancer Association Consortium (BCAC) at https://www.ccge.medschl.cam.ac.uk/breast-cancer-association-consortium-bcac/data-data-access/summary-results/gwas-summary-associations (or upon request via the BCAC Data Access Coordinating Committee at BCAC@medschl.cam.ac.uk). Related study accessions and metadata are catalogued in the GWAS Catalog under publication identifier https://www.ebi.ac.uk/gwas/publications/32424353.

The S-PrediXcan models and TWAS inputs were based on GTEx v8 expression prediction models. Recommended MASHR-based GTEx v8 eQTL prediction models and covariance files for S-PrediXcan are available from PredictDB (https://predictdb.org/) and can be downloaded from the Zenodo repository at https://zenodo.org/record/3518299 (files including mashr_eqtl.tar). Alternative Elastic Net models are available at https://zenodo.org/record/3519321.

KEGG pathway annotations and gene membership lists for the ten pathways (autophagy–animal hsa04140, endocytosis hsa04144, fatty-acid degradation hsa00071, MAPK signaling pathway hsa04010, Ras signaling pathway hsa04014, PPAR signaling pathway hsa03320, neuroactive ligand–receptor interaction hsa04080, regulation of actin cytoskeleton hsa04810, citrate cycle TCA cycle hsa00020, and synaptic vesicle cycle hsa04721) were obtained from the KEGG PATHWAY database (https://www.genome.jp/kegg/pathway.html).

The list of 35 NMN-responsive genes used for pathway nomination was taken from the reanalysis of Mills et al. (2016) reported by Cheung (2026) and is available at https://doi.org/10.6084/m9.figshare.32800638.v1.

All results generated during the current study are included in this published article and its supplementary information files.

Code availability

The analysis code used in this study is available from the corresponding author upon reasonable request.

Competing interests

The authors declare that they have no competing interests.

Funding

This research received no specific grant from any funding agency in the public, commercial, or not-for-profit sectors.

Authors' contributions

NC conceived and designed the study, performed the analyses, interpreted the results, and wrote the manuscript. All authors read and approved the final manuscript.

References

1. Bianchini G, Balko JM, Mayer IA, Sanders ME, Gianni L. Triple-negative breast cancer: challenges and opportunities of a heterogeneous disease. *Nat Rev Clin Oncol*. 2016;13:674-690. doi:10.1038/nrclinonc.2016.66
2. Zhang H, Ahearn TU, Lecarpentier J, et al. Genome-wide association study identifies 32 novel breast cancer susceptibility loci from overall and subtype-specific analyses. *Nat Genet*. 2020;52(6):572-581. doi:10.1038/s41588-020-0609-2
3. Fang EF, Lautrup S, Hou Y, Demarest TG, Croteau DL, Mattson MP, Bohr VA. NAD+ in aging: molecular mechanisms and translational implications. *Trends Mol Med*. 2017;23(10):899-916. doi:10.1016/j.molmed.2017.08.001
4. Yaku K, Okabe K, Nakagawa T. NAD metabolism: implications in aging and longevity. *Ageing Res Rev*. 2018;47:1-17. doi:10.1016/j.arr.2018.05.006
5. Mills KF, Yoshida S, Stein LR, et al. Long-term administration of nicotinamide mononucleotide mitigates age-associated physiological decline in mice. *Cell Metab*. 2016;24(6):795-806. doi:10.1016/j.cmet.2016.09.013
6. Kim J, Kundu M, Viollet B, Guan KL. AMPK and mTOR regulate autophagy through direct phosphorylation of ULK1. *Nat Cell Biol*. 2011;13(2):132-141. doi:10.1038/ncb2152
7. Lee IH, Cao L, Mostoslavsky R, et al. A role for the NAD-dependent deacetylase SIRT1 in the regulation of autophagy. *Proc Natl Acad Sci U S A*. 2008;105(9):3374-3379. doi:10.1073/pnas.0712145105
8. Cheung N. NMN prevents age-associated transcriptional drift in a tissue-dependent manner: mechanistic leads from RAB11A-mediated trafficking and CPT2-linked fatty acid oxidation [preprint]. Figshare. Published 2026. doi:10.6084/m9.figshare.32800638.v1
9. Ávalos Y, Canales J, Bravo-Sagua R, Criollo A, Lavandero S, Quest AFG. Tumor suppression and promotion by autophagy. *Biomed Res Int*. 2014;2014:603980. doi:10.1155/2014/603980
10. Morselli E, Galluzzi L, Kepp O, Vicencio JM, Criollo A, Maiuri MC, Kroemer G. Anti- and pro-tumor functions of autophagy. *Biochim Biophys Acta Mol Cell Res*. 2009;1793(9):1524-1532. doi:10.1016/j.bbamcr.2009.01.006
11. Levy JMM, Towers CG, Thorburn A. Targeting autophagy in cancer. *Nat Rev Cancer*. 2017;17(9):528-542. doi:10.1038/nrc.2017.53

12. White E. Deconvoluting the context-dependent role for autophagy in cancer. *Nat Rev Cancer*. 2012;12(6):401-410. doi:10.1038/nrc3262
13. Choi J, Jung W, Koo JS. Expression of autophagy-related markers beclin-1, light chain 3A, light chain 3B and p62 according to the molecular subtype of breast cancer. *Histopathology*. 2013;62(2):275-286. doi:10.1111/his.12002
14. Maycotte P, Gearheart CM, Barnard R, et al. STAT3-mediated autophagy dependence identifies subtypes of breast cancer where autophagy inhibition can be efficacious. *Cancer Res*. 2014;74(9):2579-2590. doi:10.1158/0008-5472.CAN-13-3470
15. Barbeira AN, Dickinson SP, Bonazzola R, et al. Exploring the phenotypic consequences of tissue-specific gene expression variation inferred from GWAS summary statistics. *Nat Commun*. 2018;9:1825. doi:10.1038/s41467-018-03621-1
16. Gamazon ER, Wheeler HE, Shah KP, et al. A gene-based association method for mapping traits using reference transcriptome data. *Nat Genet*. 2015;47(9):1091-1098. doi:10.1038/ng.3367
17. Deng Y, Pan W. A powerful and versatile colocalization test. *PLoS Comput Biol*. 2020;16(4):e1007778. doi:10.1371/journal.pcbi.1007778
18. Puri C, Vicinanza M, Ashkenazi A, et al. The RAB11A-positive compartment is a primary platform for autophagosome assembly mediated by WIPI2 recognition of PI3P-RAB11A. *Dev Cell*. 2018;45(1):114-131.e8. doi:10.1016/j.devcel.2018.03.008
19. Yu S, Yehia G, Wang J, et al. Recycling endosomes in mature epithelia restrain tumorigenic signaling. *Cancer Res*. 2019;79(16):4099-4112. doi:10.1158/0008-5472.CAN-18-3583
20. Lonic A, Gehling F, Belle L, et al. Phosphorylation of PKCδ by FER tips the balance from EGFR degradation to recycling. *J Cell Biol*. 2021;220(2):e201902073. doi:10.1083/jcb.201902073
21. Houten SM, Violante S, Ventura FV, Wanders RJA. The biochemistry and physiology of mitochondrial fatty acid β-oxidation and its genetic disorders. *Annu Rev Physiol*. 2016;78:23-44. doi:10.1146/annurev-physiol-021115-105045
22. Nowak J, Archange C, Tardivel-Lacombe J, et al. The TP53INP2 protein is required for autophagy in mammalian cells. *Mol Biol Cell*. 2009;20(3):870-881. doi:10.1091/mbc.e08-07-0671
23. You Z, Xu Y, Wan W, et al. TP53INP2 contributes to autophagosome formation by promoting LC3-ATG7 interaction. *Autophagy*. 2019;15(8):1309-1321. doi:10.1080/15548627.2019.1580510
24. Mathew R, Karp CM, Beaudoin B, et al. Autophagy suppresses tumorigenesis through elimination of p62. *Cell*. 2009;137(6):1062-1075. doi:10.1016/j.cell.2009.03.048
25. Hamurcu Z, Delibaşı N, Geçene S, et al. Targeting LC3 and Beclin-1 autophagy genes suppresses proliferation, survival, migration and invasion by inhibition of cyclin-D1 and uPAR/integrin β1/Src signaling in triple-negative breast cancer cells. *J Cancer Res Clin Oncol*. 2018;144(3):415-430. doi:10.1007/s00432-017-2557-5
26. Lefort S, Joffre C, Kieffer Y, et al. Inhibition of autophagy as a new means of improving chemotherapy efficiency in high-LC3B triple-negative breast cancers. *Autophagy*. 2014;10(12):2122-2142. doi:10.4161/15548627.2014.981788

27. Towers CG, Wodetzki D, Thorburn A. Autophagy and cancer: modulation of cell death pathways and cancer cell adaptations. *J Cell Biol*. 2020;219(1):e201909033. doi:10.1083/jcb.201909033
28. Samatar AA, Poulikakos PI. Targeting RAS-RAF-MEK-ERK signaling in cancer: promises and challenges. *Nat Rev Drug Discov*. 2014;13(12):928-942. doi:10.1038/nrd4281
29. Yaeger R, Corcoran RB. Targeting alterations in the RAF-MEK pathway. *Cancer Discov*. 2019;9(3):329-341. doi:10.1158/2159-8290.CD-18-1321
30. Imi Y, Amano R, Kasahara N, Obana Y, Hosooka T. Nicotinamide mononucleotide induces lipolysis by regulating ATGL expression via the SIRT1-AMPK axis in adipocytes. *Biochem Biophys Rep*. 2023;34:101476. doi:10.1016/j.bbrep.2023.101476
31. Sun X, Verma SP, Jia G, et al. Case-case genome-wide analyses identify subtype-informative variants that confer risk for breast cancer. *Cancer Res*. 2024;84(15):2533-2548. doi:10.1158/0008-5472.CAN-23-3854
32. Sun X, Wang M, Wang M, et al. Metabolic reprogramming in triple-negative breast cancer. *Front Oncol*. 2020;10:428. doi:10.3389/fonc.2020.00428
33. Wang Z, Jiang Q, Dong C. Metabolic reprogramming in triple-negative breast cancer. *Cancer Biol Med*. 2020;17(1):44-59. doi:10.20892/j.issn.2095-3941.2019.0210

Figures

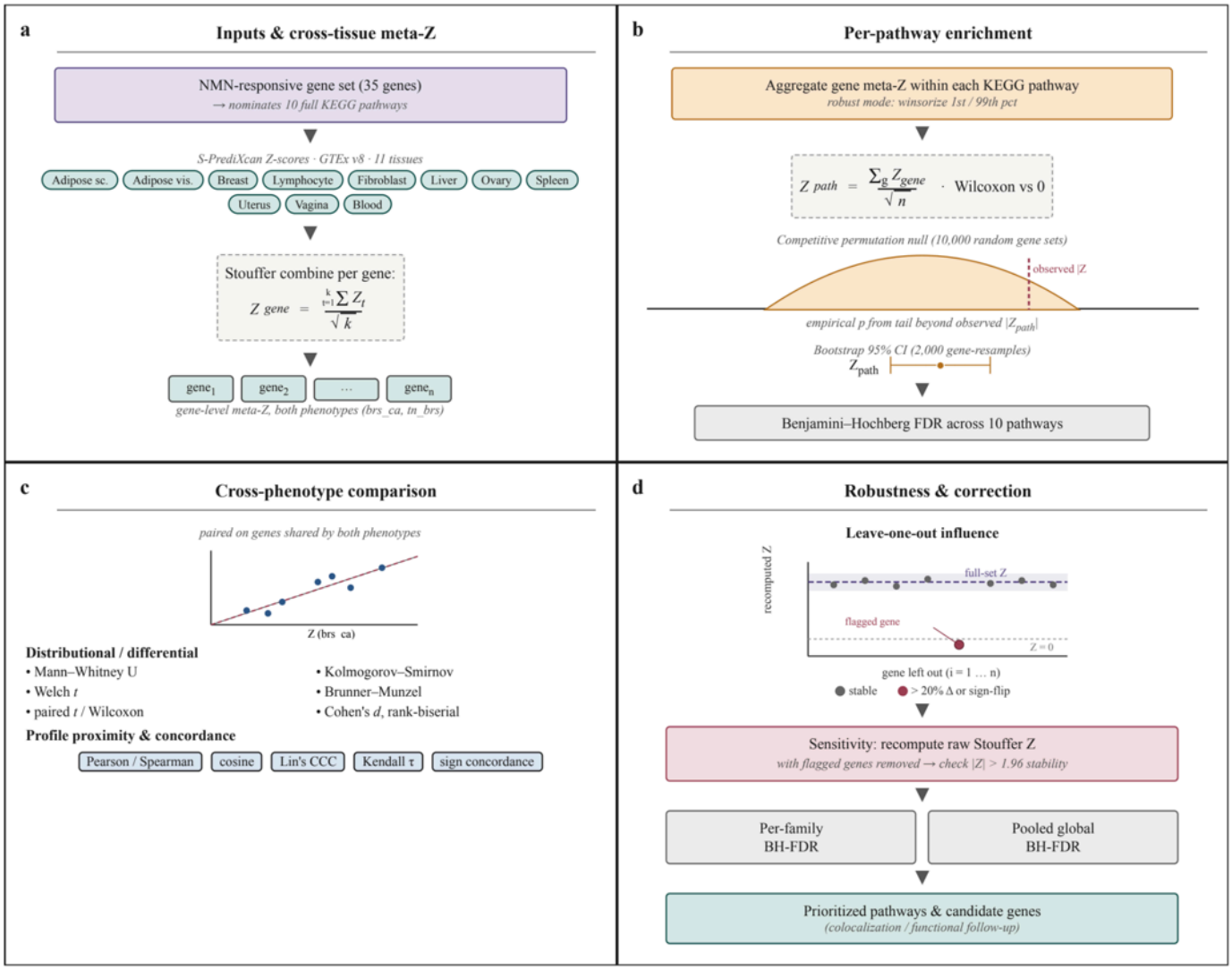


Figure 1

Overview of the multi-gene-set transcriptome-wide association (TWAS) convergence pipeline.

*Schematic of the four-stage analytical workflow applied to overall breast cancer and triple-negative breast cancer S-PrediXcan summary statistics. (**a**) Inputs and cross-tissue gene-level meta-Z construction. (**b**) Per-pathway competitive enrichment with resampling-based inference. (**c**) Cross-phenotype differential, profile-proximity, and concordance testing. (**d**) Robustness assessment via leave-one-out influence, sensitivity re-estimation, and false-discovery-rate control. Panels depict the procedure only; no results are shown.*

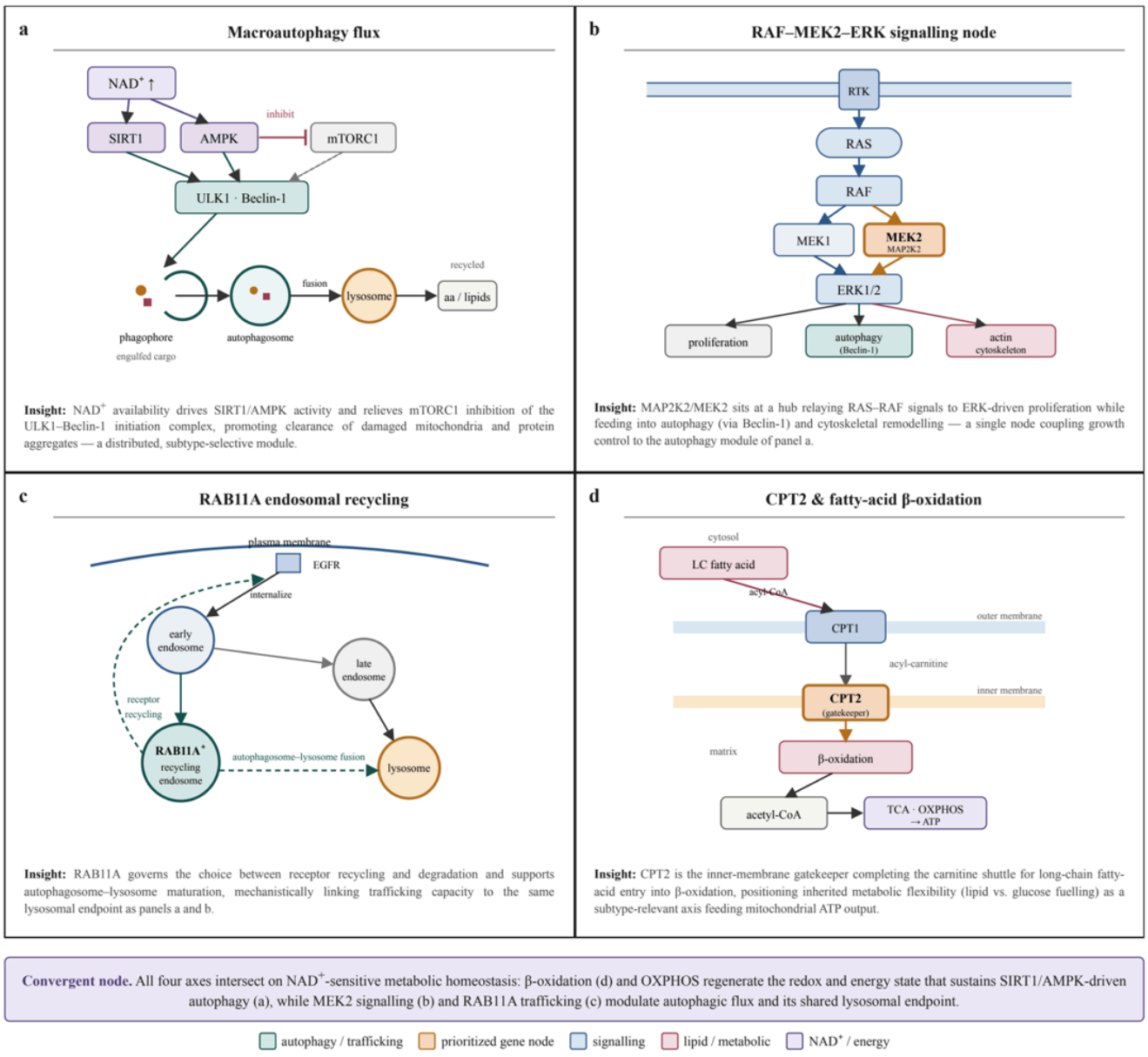


Figure 2

Candidate mechanistic axes linking NAD$^+$-responsive metabolic biology to breast-cancer-subtype vulnerability.

*Proposed molecular mechanisms underlying the four prioritized modules. (**a**) Macroautophagy and its NAD$^+$-dependent regulation. (**b**) The RAF–MEK–ERK cascade centred on MAP2K2 (MEK2) with crosstalk to autophagy and the actin cytoskeleton. (**c**) RAB11A-mediated endosomal recycling and autophagosome–lysosome maturation. (**d**) Carnitine-shuttle fatty-acid β-oxidation gated by CPT2. Diagrams depict candidate mechanisms only and do not display statistical results. Nodes shared across panels (e.g. Beclin-1, lysosome) illustrate points of pathway convergence.*

Supplementary Files

This is a list of supplementary files associated with this preprint. Click to download.

- Combined088CvDp1Appendix.docx
- GraphicalAbstract.docx